

**Study of superconducting properties and observation of c -axis superstructure
in $\text{Mg}_{1-x}\text{Al}_x\text{B}_2$**

J.Y. Xiang, D.N. Zheng*, J.Q. Li, L. Li, P.L. Lang, H. Chen, C. Dong, G.C. Che,
Z.A. Ren, H.H. Qi, H.Y. Tian, Y.M. Ni and Z.X. Zhao

*National Laboratory for Superconductivity, Institute of Physics and the Center for Condensed
Matter Physics, Chinese Academy of Sciences, Beijing 100080, PR China*

Abstract

The superconducting and structural properties of a series of $\text{Mg}_{1-x}\text{Al}_x\text{B}_2$ samples have been investigated. X-ray diffraction results confirmed the existence of a structural transition associated with the significant change in inter-boron layer distance as reported previously by Slusky *et al.* Moreover, transmission-electron-microscopy observations revealed the existence of a superstructure with doubled lattice constant along the c -axis direction. We propose that this superstructure is essentially related to the structural transition. The modifications of superconducting transition temperature T_c , the normal state resistivity, and the upper critical field B_{c2} by Al doping are discussed in terms of Al-substitution induced changes in the electronic structure at the Fermi energy.

I. Introduction

The discovery of superconductivity in magnesium diboride with a transition temperature of 39 K has attracted considerable interest [1]. This is because this metallic binary compound, which has been known since 1953 [2], consists of no transition metals and yet exhibits a remarkably high transition temperature, higher than the value obtained in any other metallic binary compounds. MgB_2 adopts a very simple hexagonal crystal structure, comprising interleaved two-dimensional boron and magnesium layers [2]. The appearance of superconductivity in MgB_2 with such a high value immediately raises the speculation for even higher superconducting temperatures in conventional metallic binary materials. On the other hand, the underline mechanism of superconductivity in this compound is still an issue of current debate. There are mainly two competitive theories that explain superconductivity in MgB_2 . The first one is based on the well-established phonon-mediated BCS theory [3], and the high T_c value is believed to be due to the high phonon frequencies and strong electron-phonon interactions. This theory is supported by the results of a number of different experiments such as isotope effect [4], quasi-particle tunnelling [5,6], specific heat [7], photoemission spectroscopy [8] and inelastic neutron scattering [9]. The second theory concerning the superconductivity in MgB_2 was put forward by Hirsch [10,11] who proposed a "universal" mechanism where superconductivity in MgB_2 was driven by the paring of dressed holes. In fact, the hole character of carriers was confirmed by Hall measurements [12].

Soon after the discovery of superconductivity in MgB_2 , Slusky *et al.* [13] reported studies of how the behavior responds to the substitution of Al for Mg in this compound. They observed that T_c decreases smoothly by a few degrees with increasing x for $0 \leq x < 0.1$ and bulk superconductivity disappears completely due to a structural instability for $x > 0.1$. In this paper, the effect of partial Al substitution for Mg on the structural and superconducting properties of MgB_2 is studied. In particular we have, for the first time, observed a superstructure in Al doped samples. We suggest that this superstructure is related to the structural transition reported by Slusky *et al.* [13]. The superconducting transition temperature, normal state resistivity and the upper critical field were also studied. The variation of these parameters with Al substitution concentration is discussed in connection with the change in structure and the density of states at the Fermi energy.

II. Experimental

Polycrystalline samples used in this study were prepared by a conventional solid reaction process. Two series of samples with similar fabrication process were made. Starting materials were elemental powders of Mg, Al and B. The raw materials with nominal composition of $\text{Mg}_{1-x}\text{Al}_x\text{B}_2$ were well mixed and pressed into discs, with 8 mm in diameter and 0.4 gram in weight. These discs were wrapped with Ta foil and sealed in quartz tubes under a background pressure about 10^{-3} Pa. The sealed quartz tubes were placed in a tube furnace, and the temperature was ramped at a rate of 100 °C per hour to 900 °C and held for two hours. This was followed by furnace cooling to the room temperature.

The microstructures and phase purity of the samples were studied by means of X-ray diffraction (XRD) and transmission electron microscopy (TEM). For TEM examination, wafers of the samples were first metallographically polished and then thinned by ion milling. Local composition was probed by energy-dispersive X-ray spectroscopy (EDX).

Resistivity measurements were made on bar-shaped samples of approximate dimensions $6 \times 3 \times 2$ mm using a four-probe technique with a current of 10 mA. AC-susceptibility measurements were also performed to determine the superconducting transition temperature. DC-magnetization was measured in a Quantum Design SQUID magnetometer.

III. Results and discussion

The X-ray powder diffraction patterns obtained on the samples showed the predominant phase was of MgB_2 type and there were some minor amount of impurity phases such as MgO presented in the samples. The partial representation of the XRD patterns in the 2θ range of 50 to 60 degree is shown in Fig.1. The results are similar to that reported by Slusky *et al.* [13], *i.e.*, the substitution of Al results in a significant change in the c -axis lattice parameter while the in-plane lattice parameter is relatively constant. In the range between $x=0.09$ to $x=0.2$, the (002) reflection peak becomes broad, indicating the partial collapse of the separation between boron sheets and the presence of two isostructure phases. Figure 2 shows the lattice parameters as a function of Al substitution level. In the shadowed region, because of the peak broadening, there is a large uncertainty associated with the value of c . Nevertheless, the data in Fig.2 show that in the shadowed region there appears a discontinuity, which could be related to a structural transition as pointed out in Ref .13.

In Fig.3, we show the normal state resistivity as a function of Al concentration. Because of the porous nature of the sintered ceramic samples, the resistivity cannot be determined accurately and the data are somewhat scattering. Nevertheless, as shown in Fig 3, there is clearly trend that the normal state resistivity increases with increasing Al concentration. This increase is compatible with the reduction of hole carriers in the samples with Al substitution. The increase of the normal state resistivity upon Al substitution has also been reported by Lorenz *et al.* for doping level up to $x=0.1$ [14] although the magnitude of increase in resistivity ($\sim 100\%$ from $x=0$ to 0.1) is greater than that shown in Fig.3 ($\sim 50\%$ from $x=0$ to 0.1). This is probably due to the difference in porosity and grain boundary scattering of the two sets of samples.

In Fig.4, we show the variation of superconducting transition temperature T_c as a function of Al substitution level. The T_c values were determined from the temperature dependence of DC magnetization curves measured on bar-shaped samples. The data show clearly that as Al content increases T_c decreases progressively. Also, there appear two regions in which T_c varies differently with x . The change of T_c with x is slower in the low Al doping region ($x < 0.1$) than in the high Al doping region ($x > 0.1$). The $x=0.1$ composition coincides approximately with the substitution level at which two-phase region appears. As pointed out by Slusky *et al.*[13], the compound MgB_2 is near a structural instability, at slightly higher electron concentration, that can destroy the superconductivity. At high substitution levels, bulk superconductivity is destroyed due to the presence of a non-superconducting isostructure phase. We suggest that the relatively fast drop of T_c in the region of $x > 0.1$ is probably resulted from the suppression of the bulk superconductivity.

On the other hand, the decrease of T_c at substitution levels lower than $x=0.1$ has been attributed to a density of states effect [13,14]. In MgB_2 the Fermi energy E_F is close to an edge of rapidly decreasing density of states and any increase of E_F by Al substitution could result in a significant decrease of the density of states at Fermi energy $N(E_F)$, which, in the BCS formulism, leads to a decrease of T_c . In the next few paragraphs, we present the results of the upper critical field B_{c2} and try to deduce some information concerning $N(E_F)$.

In the inset of Fig.5 magnetic moment versus temperature curve measured at 0.5 T for the $x=0.07$ sample is shown. A small normal state background contribution has been subtracted from the data. Like commonly observed in high- T_c superconductors, there were two

characteristic temperatures T_c and T_{irr} . In the region between these two temperatures, field-cooled (FC) and zero-field-cooled (ZFC) magnetization data were overlapped. The superconducting transition temperature was defined as the intercept of a linear extrapolation of the magnetic moment in the superconducting state with the normal state base line. The field dependence of T_c gives the upper critical field B_{c2} data, which are presented in Fig.5 for the two samples with $x=0$ and $x=0.07$, respectively. For both samples, B_{c2} shows approximately linear temperature dependence with a slope of -0.6 T/K and -0.58 T/K, respectively. For the $x=0$ sample, the value is similar to that reported in the literature [15]. The zero-temperature value of upper critical field $B_{c2}(0)$ is estimated using the formula [16];

$$B_{c2}(0) = -0.7 \left. \frac{\partial B_{c2}}{\partial T} \right|_{T_c} . \quad (1)$$

Application of Eq.(1) to the experimental data yields $B_{c2}(0)$ values of 16.2 T for $x=0$ and 14.8 T for $x=0.07$. Clearly, the decrease of $B_{c2}(0)$ is primarily due to the decrease of T_c and the slope is barely changed.

As discussed above, the band calculation showed that in MgB_2 the Fermi energy is situated around a peak in the density of states [3,18,19]. The substitution of Al increases the electron transfer from the Mg plane. In a rigid band picture, this would mean a decrease of the density of states at the Fermi energy $N(E_F)$. In the BCS framework, $N(E_F)$ can be related to the slope of B_{c2} near T_c with the relation $-(dB_{c2}/dT)_{T_c} \sim \mathbf{r}N(E_F)$, where \mathbf{r} is the residual normal state resistivity. The variation of $(dB_{c2}/dT)_{T_c}$, as indicated in Fig.5, is less than 10% for the doping level up to $x=0.07$ while the normal state resistivity increases by a large magnitude as shown in Fig.3 (around 40% for $x=0.07$). Therefore the increase of \mathbf{r} with increasing the Al concentration level can qualitatively account for the decrease of the density of state at the Fermi level. If the resistivity can be measured more accurately, a more quantitative estimation of $N(E_F)$ may be made.

In order to characterize the structural features associated with the structural transition as reported in present system, we have carried out TEM investigations on the Al doped samples, especially, with x ranging from 0.1 to 0.25. As a result, a variety of structural phenomena have been revealed in these materials, such as phase separation and intergrowth of two structural phases. The most strike structural feature found in this investigation is the presence of a superstructure phase of doubled lattice parameter along the c -axis direction. Figure 6 presents the electron diffraction patterns for two samples taken along the b -axis direction. Figure 6a is the electron diffraction pattern of the pure MgB_2 sample, all diffraction spots can be well

indexed by the hexagonal cell with lattice parameters of $a=0.307$ nm and $c=0.357$ nm. The pattern in Fig.6b was taken on a $x=0.25$ sample. In addition to the basic reflection spots, evident superstructure spots can be clearly recognized at the systematic $(h, k, l + 1/2)$ positions. TEM examination also revealed that the grains were very small, on the order of 0.1μ in the $x=0.25$ sample. It would be desirable to fabricate samples with larger grains that would allow more detailed TEM study. Work along this line is undergoing. Nevertheless, we could see that the phase with the superstructure intergrows with the normal MgB_2 phase. Presumably, the phase with the superstructure is non-superconducting and the bulk superconductivity is destroyed when the phase is presented and separates the crystalline grains into small superconducting regions.

The superstructure, however, was not observed in XRD spectra. In principle, the appearance of the superstructure with doubled c -axis parameter would result in an additional $(00l)$ peak at low 2θ angle. The XRD data showed no sign of such a peak within the instrumental sensitivity. We believe this is due to the very similar X-ray scattering factor for Mg and Al atoms. The diffraction of X-ray by atoms in a crystal lattice is due to the interaction between the surrounding electrons and X-ray. Mg and Al are elements that occupy positions next to each other in the periodic table, and the electron cloud distribution is very similar for Mg^{2+} and Al^{3+} . Therefore the scattering factor is almost the same for the two elements. Furthermore, the phase with superstructure is presented in small regions, especially for the low Al doped samples, and hence the XRD peak may become smearing and difficult to be observed. On the other hand, TEM can probe the structure in a comparatively small region. Moreover, the diffraction of charged electrons is more sensitive to the electric field potential of atoms that are different for Mg and Al atoms. Thus, the superstructure can be observed more readily by TEM.

In order to ensure that the observed superstructure is resulted from Al substitution, we made a systematical examination on two sets of samples with $0 \leq x \leq 1$. The results indicate that this superstructure appears in a large range with $0.1 \leq x \leq 0.7$ together with both Al ordering and the resultant structural distortion. A more detailed analysis about atomic structure in this superstructure phase will be reported in a forthcoming paper [20].

In summary, we have investigated the effect of Al substitution for Mg on the structural and superconducting properties of $\text{Mg}_{1-x}\text{Al}_x\text{B}_2$ samples. The X-ray diffraction results

confirmed the existence of a structural transition associated with the significant change in inter-boron layer distance as reported previously by Slusky *et al.*[13]. Moreover, transmission electron microscopy examination showed the existence of a superstructure in the direction perpendicular to the boron honeycomb layers with doubled c -axis lattice parameter. We propose that the observed superstructure is related to the previously reported structural transition. The experimental results showed that the normal state resistivity was increased and T_c was decreased with increasing the Al concentration, respectively. The upper critical field B_{c2} was determined for samples with low Al concentrations and found to be reduced by Al doping. Furthermore, an estimation of the density of states at the Fermi energy $N(E_F)$ using the B_{c2} and normal state resistivity data suggests that $N(E_F)$ is decreased too, being consistent with theoretical calculations.

Acknowledgements

The work is supported by the National Center for Research and Development on Superconductivity and the Ministry of Science and Technology (NKBRSF-G19990646). One of us (JQL) acknowledges the support of ‘Hundred of Talents’ program organized by the Chinese Academy of Sciences, P.R. China.

Reference

* Corresponding author, E-mail: Dzheng@ssc.iphy.ac.cn

1. J. Nagamatsu, *et al.* *Nature*. **410**, 63-64(2001).
2. M.E. Jones & R.E. Marsh, *J. Amer. Chem. Soc.* **76** 1434(1954).
3. J. Kortus, *et al.* *cond-mat/0101446* (2001).
4. S.L. Bud'ko, *et al.* *Phys. Rev. Lett.* **86**, 1877(2001).
5. H. Schmidt, *et al.* *cond-mat/0102389*(2001).
6. A. Sharoni, *et al.* *cond-mat/0102325*(2001).
7. R.K. Kremer, *et al.* *cond-mat/0102432* (2001).
8. T. Takahashi, *et al.* *cond-mat/0103079* (2001).
9. T. Yildirim, *et al.* *cond-mat/0103469* (2001).
10. J.E. Hirsch . *cond-mat/0102115*.(2001)
11. J.E. Hirsch & F. Marsiglio. *cond-mat/0102479*.(2001)
12. W.N. Kang, *et al.* *cond-mat/0102313*(2001).
13. J.S. Slusky, *et al.* *Nature*. **410**, 343(2001).
14. B. Lorenz, *et al.* *cond-mat/0104041*(2001).
15. D. K. Finnemore, *et al.* *Phys. Rev. Lett.* **86**, 2420(2001).
16. N.R. Werthamer, E. Helfand & P.C. Hohenberg. *Phys. Rev.* **147**, 288(1966).
17. D.R. Armstrong, *et al.* *J. Chem. Soc. Faraday. Trans.* **275**, 13(1979)
18. A.L. Ivanovskii, *et al.* *Russ. J. Inorg. Chem.* **45**, 1234(2000).
19. J.Q. Li, *et al.* to be published.

Figure captions

Figure 1 Partial representation of X-ray diffraction patterns for a series of $\text{Mg}_{1-x}\text{Al}_x\text{B}_2$ samples.

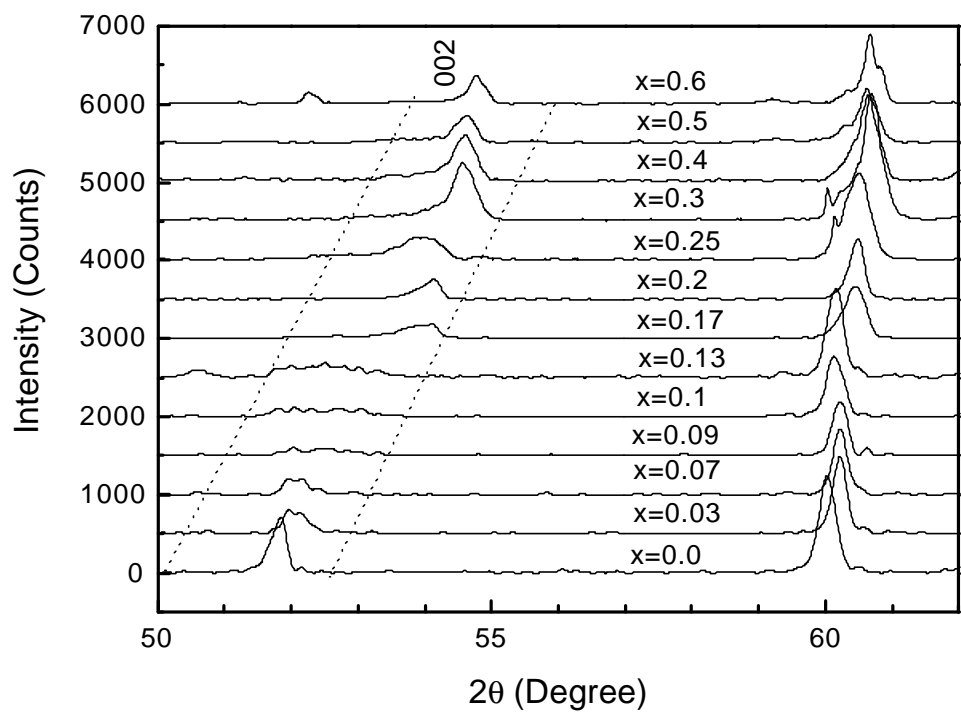
Figure 2. The lattice parameter a and c as a function of Al concentration. In the shadowed region, the (002) reflection peak is broad, indicating the partial collapse of the separation between boron layers.

Figure 3. The normal state resistivity measured at 40 K versus Al concentration.

Figure 4. Variation of the superconducting transition temperature T_c with Al concentration.

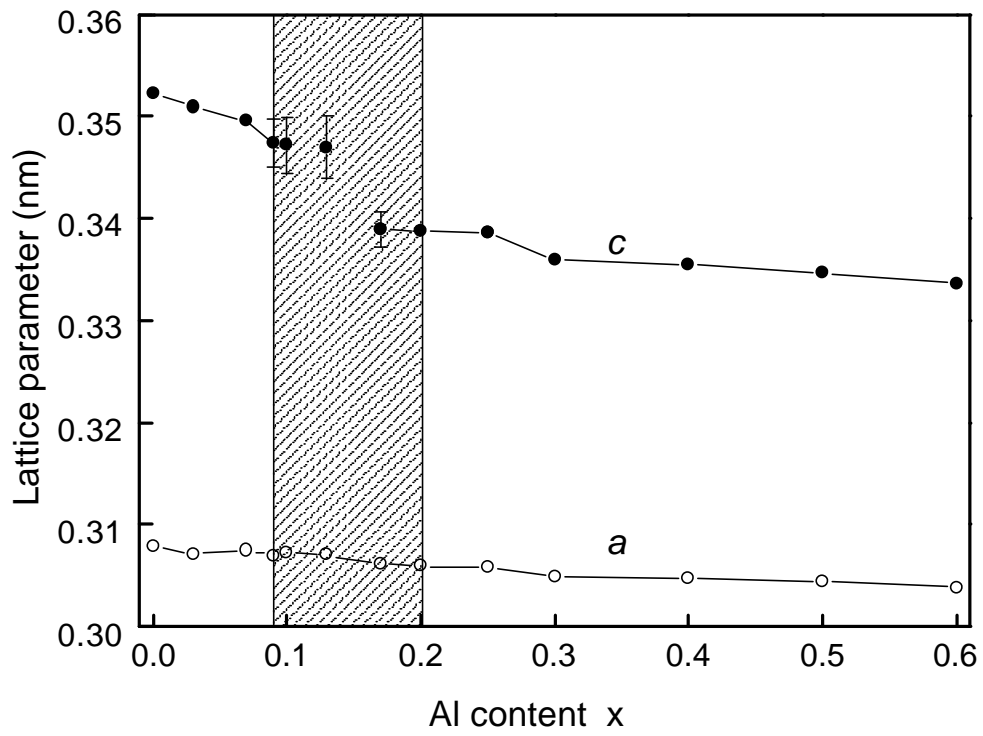
Figure 5. Temperature dependence of the upper critical field B_{c2} for the $x=0$ and 0.07 samples. The inset shows the FC and ZFC magnetization data as a function of temperature measured at 0.5 T for the $x=0.07$ sample. The superconducting transition temperature T_c and the irreversibility temperature T_{irr} are indicated in the graph.

Figure 6. TEM diffraction patterns for the two $\text{Mg}_{1-x}\text{Al}_x\text{B}_2$ samples. a) $x=0$, b) $x=0.25$.



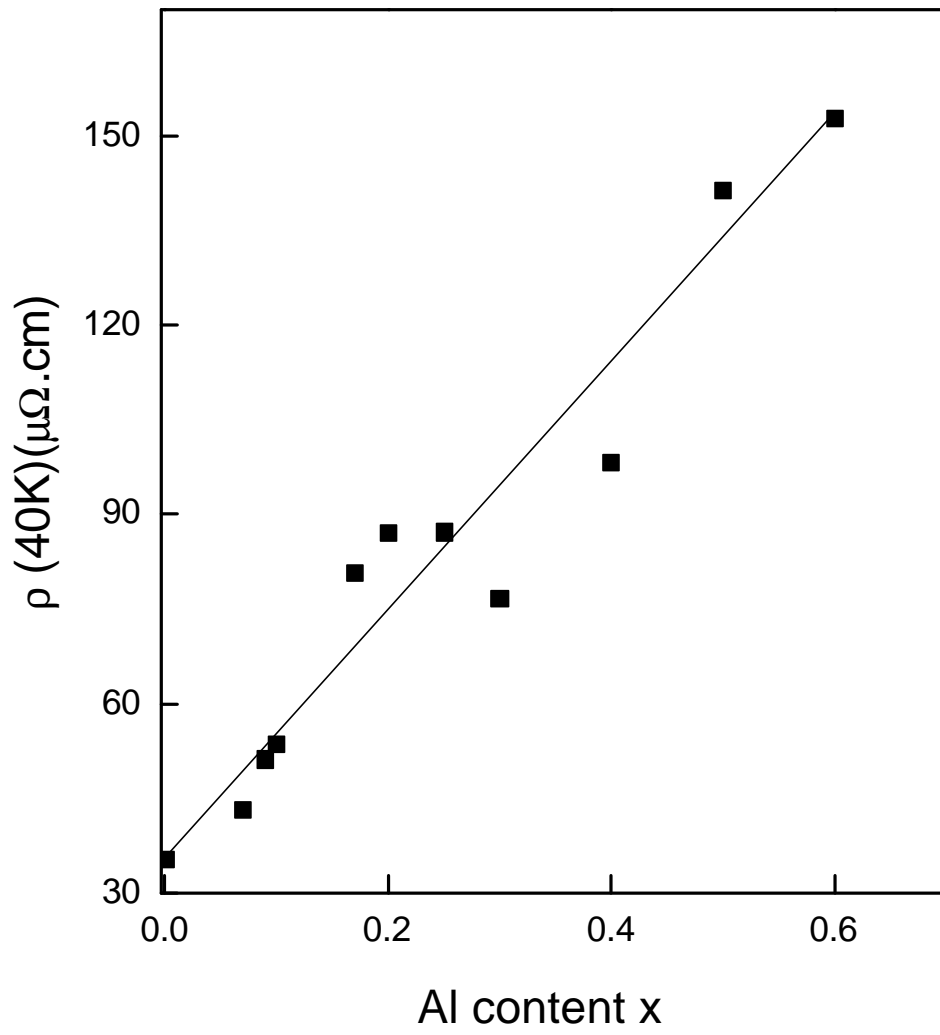
Xiang et al

Figure 1

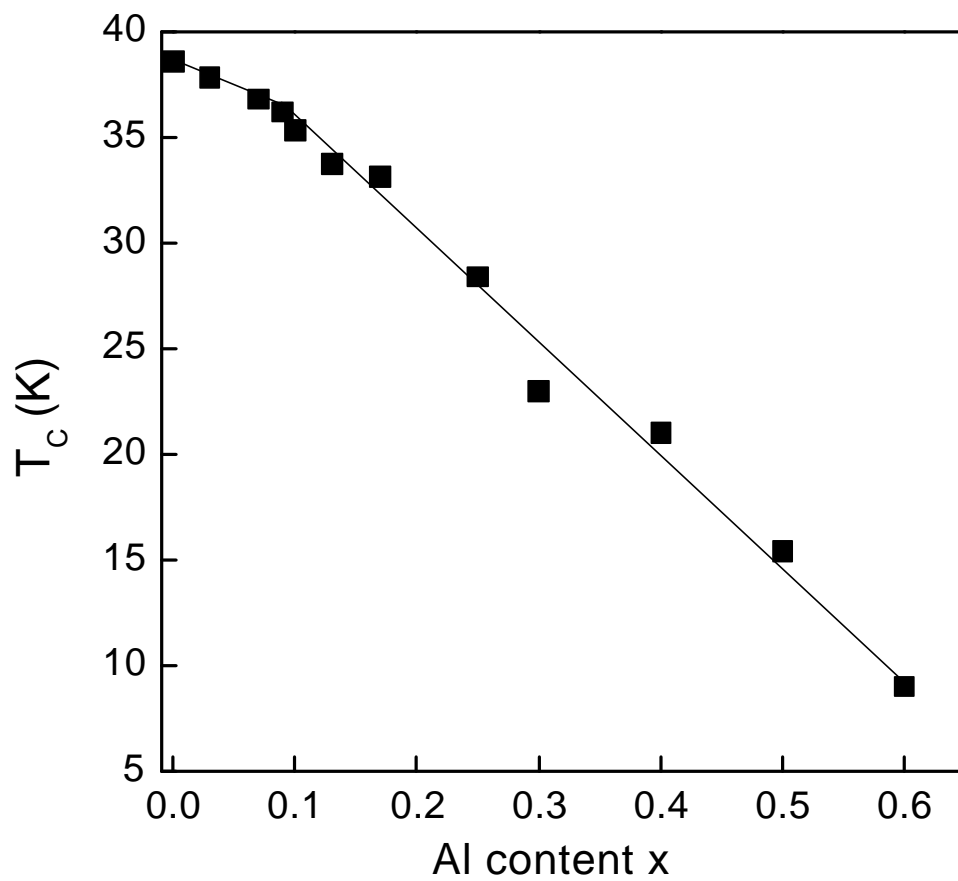


Xiang et al

Figure 2

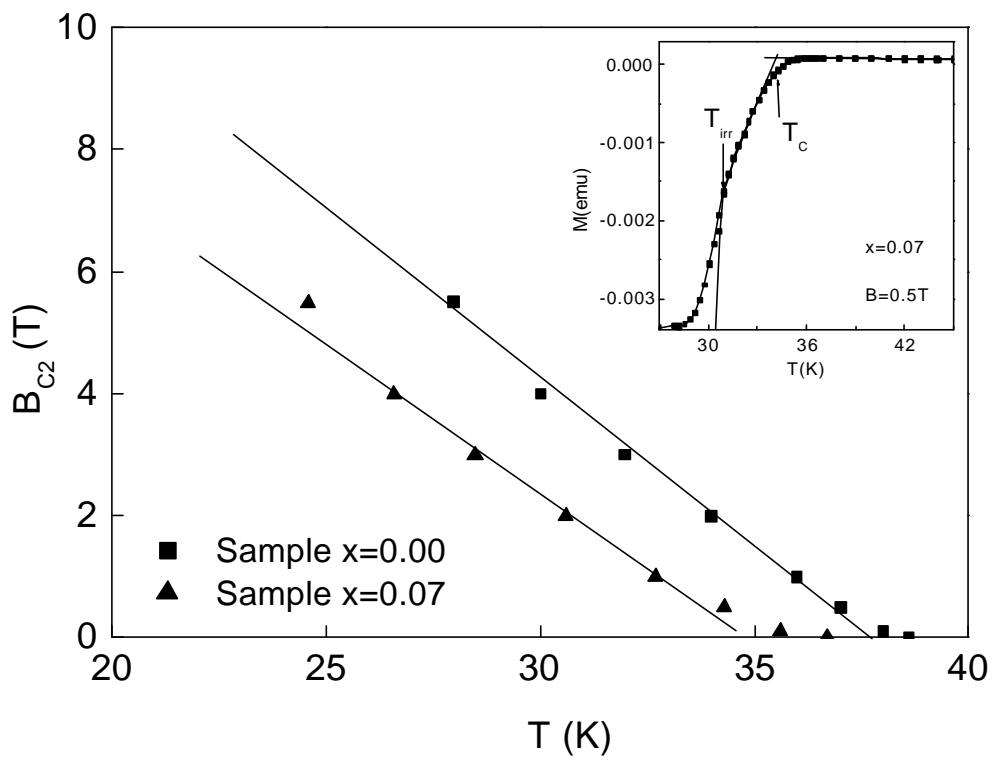


Xiang et al. Figure 3



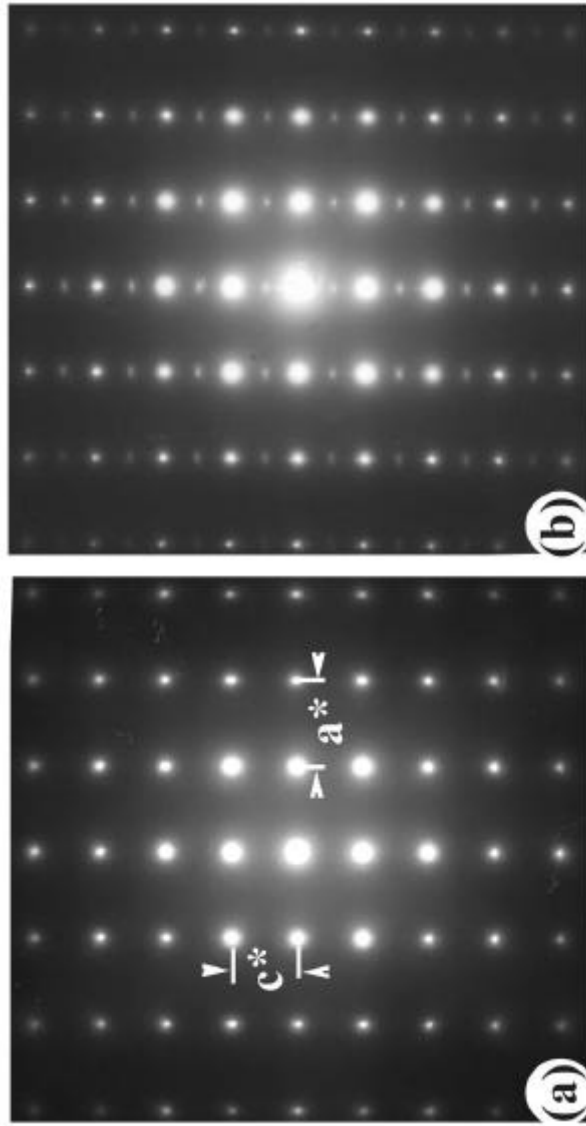
Xiang et al.

Figure 4



Xiang et al

Figure 5



Xiang et al

Figure 6